Annu. Rev. Fluid Mech. 1997. 29:399–434

BLOOD FLOW IN ARTERIES

David N. Ku
G. W. Woodruff School of Mechanical Engineering, Georgia Institute of Technology, Atlanta, Georgia 30332-0405

ABSTRACT

Blood flow in arteries is dominated by unsteady flow phenomena. The cardiovascular system is an internal flow loop with multiple branches in which a complex liquid circulates. A nondimensional frequency parameter, the Womersley number, governs the relationship between the unsteady and viscous forces. Normal arterial flow is laminar with secondary flows generated at curves and branches. The arteries are living organs that can adapt to and change with the varying hemodynamic conditions. In certain circumstances, unusual hemodynamic conditions create an abnormal biological response. Velocity profile skewing can create pockets in which the direction of the wall shear stress oscillates. Atherosclerotic disease tends to be localized in these sites and results in a narrowing of the artery lumen—a stenosis. The stenosis can cause turbulence and reduce flow by means of viscous head losses and flow choking. Very high shear stresses near the throat of the stenosis can activate platelets and thereby induce thrombosis, which can totally block blood flow to the heart or brain. Detection and quantification of stenosis serve as the basis for surgical intervention. In the future, the study of arterial blood flow will lead to the prediction of individual hemodynamic flows in any patient, the development of diagnostic tools to quantify disease, and the design of devices that mimic or alter blood flow. This field is rich with challenging problems in fluid mechanics involving three-dimensional, pulsatile flows at the edge of turbulence.

INTRODUCTION

The cardiovascular system primarily functions in nutrient and waste transport throughout the body. The heart pumps blood through a sophisticated network of branching tubes. The blood vessels distribute blood to different organs and supply themselves with nutrition. The arteries, far from inert tubes, adapt to varying flow and pressure conditions by enlarging or shrinking to meet changing hemodynamic demands.

0066-4189/97/0115-0399$08.00

Blood flow under normal physiologic conditions is an important field of study, as is blood flow under disease conditions. The majority of deaths in developed countries result from cardiovascular diseases, most of which are associated with some form of abnormal blood flow in arteries. Many investigators have made seminal contributions to this field, but their work cannot all be cited because of page limitations. Instead, this review focuses on selected areas of cardiology and vascular surgery by first discussing basic normal flows in arteries and the biological responses to these flows. Then the review examines flows through stenoses and the importance of their fluid mechanics to clinical medicine.

PHYSIOLOGIC ENVIRONMENT

Blood is a complex mixture of cells, proteins, lipoproteins, and ions by which nutrients and wastes are transported. Red blood cells typically comprise approximately 40% of blood by volume. Because red blood cells are small semisolid particles, they increase the viscosity of blood and affect the behavior of the fluid. Blood is approximately four times more viscous than water. Moreover, blood does not exhibit a constant viscosity at all flow rates and is especially non-Newtonian in the microcirculatory system. The non-Newtonian behavior is most evident at very low shear rates when the red blood cells clump together into larger particles. Blood also exhibits non-Newtonian behavior in small branches and capillaries, where the cells squeeze through and a cell-free skimming layer reduces the effective viscosity through the tube. However, in most arteries, blood behaves in a Newtonian fashion, and the viscosity can be taken as a constant, 4 centipoise. Non-Newtonian viscosity is extensively studied in the field of biorheology and has been reviewed by others (e.g. Chien 1970, Rodkiewicz et al 1990).

Blood flow and pressure are unsteady. The cyclic nature of the heart pump creates pulsatile conditions in all arteries. The heart ejects and fills with blood in alternating cycles called *systole* and *diastole*. Blood is pumped out of the heart during systole. The heart rests during diastole, and no blood is ejected. Pressure and flow have characteristic pulsatile shapes that vary in different parts of the arterial system, as illustrated in Figure 1. The flow out of the heart is intermittent, going to zero when the aortic valve is closed. The aorta, the large artery taking blood out of the heart, serves as a compliance chamber that provides a reservoir of high pressure during diastole as well as systole. Thus the blood pressure in most arteries is pulsatile, yet does not go to zero during diastole. In contrast, the flow is zero or even reversed during diastole in some arteries such as the external carotid, brachial, and femoral arteries. These arteries have a high downstream resistance during rest and the flow is essentially on/off with each cycle. In other arteries such as the internal carotid

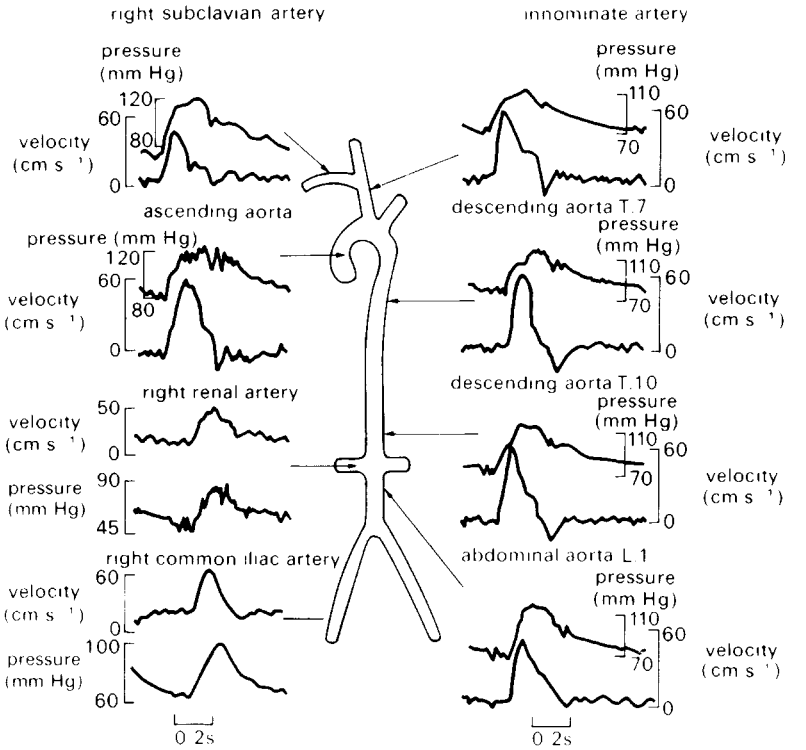

Figure 1 Pressure and velocity pulse waveforms in the aorta and arterial branches of a dog. Note that the pressure maximum becomes amplified while the velocity maximum decreases as the blood moves downstream. (From Caro et al 1978, *The Mechanics of the Circulation*; reprinted by permission of Oxford University Press.)

or the renal arteries, the flow can be high during diastole if the downstream resistance is low. The flow in these arteries is more uniform.

GENERAL FLUID MECHANICAL CONSIDERATIONS

The existence of unsteady or pulsatile flow virtually throughout the cardiovascular system forces the inclusion of a local acceleration term in most analyses. The typical Reynolds number range of blood flow in the body varies from 1 in small arterioles to approximately 4000 in the largest artery, the aorta. Thus the flow spans a range in which viscous forces are dominant on one end and inertial forces are more important on the other.

A dimensional analysis of the unsteady Navier-Stokes equations leads to a nondimensional number commonly referred to as the Womersley or Witzig

parameter:

$$\alpha = R\sqrt{\frac{\omega}{\nu}},$$

where R is the tube radius, ω is the angular frequency, and ν is the kinematic viscosity (Womersley 1955). This parameter is used in the similarity transform developed in the well-known Stokes' Second Problem, in which flow is induced by an oscillating flat plate.

The Womersley parameter α can be interpreted as the ratio of the unsteady forces to the viscous forces. When the Womersley parameter is low, viscous forces dominate, velocity profiles are parabolic in shape, and the centerline velocity oscillates in phase with the driving pressure gradient (Womersley 1955, McDonald 1974). For Womersley parameters above 10, the unsteady inertial forces dominate, and the flow is essentially one of piston-like motion with a flat velocity profile. The amplitude of motion decreases at the higher frequencies, and there is a 90° phase difference between the pressure gradient and flow, as in a low-pass filter.

In contrast to unsteadiness, several features of biological flows may be neglected in some situations as secondary in importance. These properties include vessel wall elasticity, non-Newtonian viscosity, slurry particles in the fluid, body forces, and temperature. Although each is physiologically relevant, the analysis is greatly simplified when these can be justifiably neglected, which is the case in most arterial flows.

One-Dimensional Models

Pressure and flow have characteristic pulsatile shapes that vary in different parts of the arterial system, as illustrated in Figure 1. The relationship between the pressure waveform and total blood flow can be explained through a global analysis of the fluid mechanics. The entire cardiovascular system may be simplified using a lumped parameter or one-dimensional (1D) model of flow. The most well-known model is that of the Windkessel (shown in Figure 2), which has been used to explain the rapid rise and gradual decrease of the flow and pressure waveforms (e.g. McDonald 1974).

The Windkessel model describes the cardiovascular system in terms of a compliant section in series with a resistive section. During systole, the compliant aorta acts like a capacitor to store blood. During diastole, the elastic aorta discharges the stored blood through the resistive branches of the smaller arteries to various organs. The pressure and flow waveforms given by this model are quite close to those measured in the body. Other investigators have produced more elaborate models with many elements in order to refine the waveform predictions (Nichols & O'Rourke 1990). The lumped parameter approach is

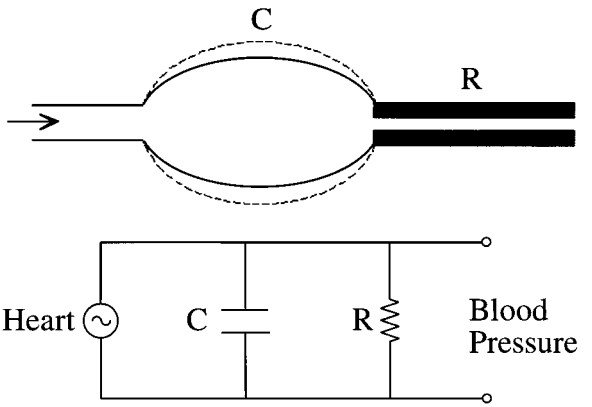

Figure 2 A lumped-parameter model of the arterial system. (*Upper*) Lumped fluid mechanics elements for arterial capacitance and resistance of the elastic aorta. (*Lower*) Conventional electrical element Windkessel model, where R is the flow resistance and C is the capacitance created by the elastic aorta.

useful for an understanding of the physiology of measured waveforms, afterload impedance, and work by the heart during ejection. This approach can also be used to determine variations in local blood flow distribution that may occur at branch points (Holenstein & Ku 1988) or within tumors (Eskey et al 1994). One-dimensional differential models of flow in an elastic blood vessel also describe pulse wave propagation and wavespeeds (McDonald 1974). In addition, these models are useful in providing outlet boundary conditions for computational fluid dynamics.

Velocity Profiles

Vascular biologists are currently more concerned with the local hemodynamic conditions in a given artery or branch than simply the flow waveform predicted by IO models. A detailed local description of these pulsatile flows is needed. The fluid-wall shear stress in a blood vessel for a given pulsatile flow situation often needs to be determined. Fully developed pulsatile flow in a straight or tapered tube can be expressed analytically (Womersley 1955). A physiologic pressure or flow waveform can be expanded as a Fourier series, and the harmonic components of velocity can be summed to yield the unsteady velocity profiles. Although in the past this summation was carried out by hand with tables, now it can be easily calculated using a simple computer program such as Mathematica (He et al 1993). Figure 3 shows an example of velocity profiles for a femoral artery of a dog. The Womersley solution for velocity can be used to generate excellent approximations for shear stress as long as secondary and

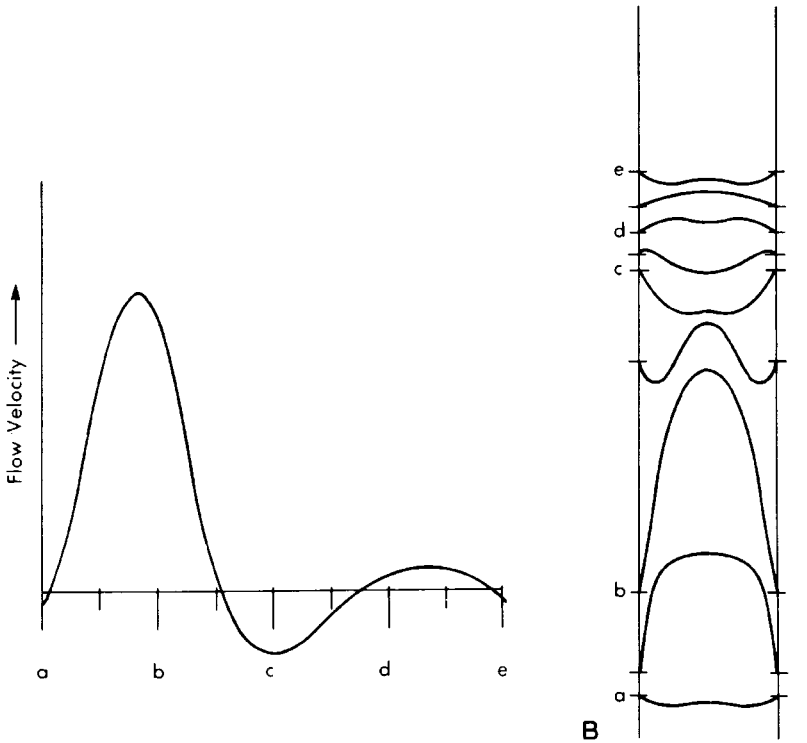

Figure 3 (*A*) Flow velocity waveform in a normal femoral arterial flow. (*B*) The velocity profiles are obtained from the analysis given by Womersley for pulsatile flow in a straight, rigid tube. Various velocity profiles are evident through the cardiac cycle. Lower velocity at the wall is the first to reverse direction. (Reprinted with permission of W. B. Saunders Company.)

separated flows are not present. Analytical solutions have also been obtained for flow through arteries that translate or change their radius of curvature, such as coronary arteries, which ride on the moving heart surface (Delfino et al 1994).

Entrance Regions

Flow from the heart comes from a large pressure reservoir into successively smaller tubes. The flow is not fully developed near some of the origins of arteries. Flow in these regions is similar to an entrance flow with a potential core and a developing boundary layer at the wall. The velocity profiles are blunt near the center, and the centerline velocity accelerates as the boundary layer retards velocity near the wall.

Unsteady flow through the entrance region depends on the Womersley parameter as well as the Reynolds number. For low Womersley parameters, the maximum unsteady entrance length is approximately the same as the steady entrance length for the peak flow and is primarily dependent on the Reynolds number. For high Womersley parameters, the Stokes boundary layer growth is faster and the entrance length is more uniform during the cycle. For $\alpha \geq 12.5$, the pulsatile entrance length is approximately the same length as the entrance length of the mean flow. At all α, the wall shear rate converges to its fully developed value at about half the length at which the centerline velocity converges to its fully developed value. Thus the upstream flow conditions leading to a specific artery may or may not be fully developed and can be predicted by the magnitudes of the Reynolds number and Womersley parameter (He & Ku 1994).

Although a Womersley-type analysis is useful to gain a general understanding of the relevant forces, the nonlinear convective term is important to many flows at arterial branches. Likewise the flow in most arteries is subject to viscous forces that cannot be neglected. For a medium-sized artery, the Reynolds number is typically on the order of 100 to 1000, and the Womersley parameter ranges from 1 to 10 (Caro et al 1978). These conditions allow for few simplifications of the unsteady Navier-Stokes equations. Arteries have a high degree of stiffness that does allow for a long wavelength approximation. In most cases, the effects of elasticity are very small, so that an assumption of rigid tube flow is reasonable. Most studies of artery hemodynamics use experimental measurements, potential flow theory, or computational fluid mechanics. The three-dimensional (3D) nature of many of these unsteady flows is a serious obstacle to computational methods because the computational time required is enormous.

Measurement Techniques

Much of our hemodynamics knowledge comes from a range of experiments that recreate the unsteady, 3D flow in laboratory models. Most of the standard fluid mechanics techniques have been applied to these models. Particle tracking velocimetry, hydrogen bubbles, dye streaklines, photochromic lines, and dye washout give excellent pictures of the physical 3D flow structures, as in Figure 4 (e.g. Karino & Goldsmith 1979, Ku & Giddens 1983, Ohja et al 1990, Keynton et al 1991). Hot-film anemometry, laser Doppler anemometry, and pulsed Doppler ultrasound have been used to make detailed velocity profiles in other models (Nerem & Seed 1972, Friedman et al 1980, Khalifa & Giddens 1981, Ku & Giddens 1987). More recently, magnetic resonance velocimetry has gained popularity (Meier et al 1988, Ku et al 1990a, Kim et al 1995). These measurements verify the general fluid dynamic picture of the unsteady flows described above and have led to the detailed knowledge of blood flow at specific arteries given below.

Figure 4 Hydrogen bubble visualization of flow through a model carotid bifurcation illustrating the laminar flow at the flow divider and separation of flow at the posterior wall of the internal carotid sinus. The separation region of transient reverse velocities is also the site of secondary vortex patterns. (Reprinted by permission of the American Heart Association, Inc.)

Curved Tubes

The main systemic artery from the heart is the aortic arch, which is a 3D bend twisting through more than 180°. Flow in a curved tube flow was analyzed by Dean (1928), who developed a parameter relating the centrifugal forces to the viscous forces. The Dean number is basically a combination of the Reynolds number and the nondimensional ratio of tube radius to radius of curvature.

$$\text{Dean number} = (2\delta)^{1/2} \cdot 4Re,$$

where $\delta = \dfrac{\text{radius of tube cross section}}{\text{radius of curvature of the centerline}}$ and Re is the Reynolds number.

By convention, the Dean number includes a few numerical constants (Pedley 1980).

Two basic flow conditions exist within the aortic arch. If flow into the entrance of the tube is not developed, then the core of the fluid in the curve can act like a potential vortex with velocity skewing toward the inner wall. Fully developed flow upstream of or through curved tubes exhibits velocity that skews toward the outer wall of the bend. For most arterial flows, skewing will be toward the outer wall. Secondary flow develops as counter-rotating vortices with flow in the middle that moves toward the outer wall. With higher Dean numbers, flow can separate along the inner curve. Pulsatile flow through a curved tube can induce complicated secondary flows with flow reversals. An extensive discussion of curved tube flows is available in the book by Pedley (1980).

Separated Flows

A few locations in the arterial system have expansion regions. The cross-sectional area along the axis may enlarge at sinuses and aneurysms. At these anatomic structures, the change in area must be included in the continuity equation as:

$$\bar{u}A = Q(t).$$

One can use the 1D, unsteady Euler equation to get an estimate of the local pressure changes for a given area enlargement:

$$\frac{\partial \bar{u}}{\partial t} + \bar{u}\frac{\partial \bar{u}}{\partial x} = -\frac{1}{\rho}\frac{\partial p}{\partial x}.$$

Some rearranging yields a single equation:

$$\frac{\partial p}{\partial x} = -\frac{\rho}{A}\frac{dQ}{dt} + \frac{\rho Q^2}{A^3}\frac{dA}{dx}.$$

From this equation, one can see that a favorable (negative) pressure gradient exists when the flow is accelerating (dQ/dt is positive) and the area is converging (dA/dx is negative). However, if the area is diverging and the flow is

decelerating, an adverse pressure gradient can exist. In this situation, flow separation is possible and typically occurs along the walls of the aneurysm (Taylor & Yamaguchi 1994). Dimensional values can be assigned to the constants for a particular arterial situation such as the carotid sinus for a given pulsatile flow. Transient separation can then be predicted to occur at this branch (Giddens & Ku 1987).

Shear Stress

As blood flows across the endothelium, a shear stress is generated to retard the flow. The wall shear stress is proportional to the velocity gradient at the wall and the fluid viscosity:

$$\tau = \mu\, du/dr.$$

Shear stress for laminar steady flow in a straight tube is expressed as

$$\tau_{wall} = \frac{32\mu Q}{\pi D^3}$$

and is a reasonable estimate of the mean wall shear stress in arteries. In situations where the lumen is not circular or the blood flow is highly skewed, as at branch points, shear stress can vary widely and may be determined through detailed measurements of velocity near the wall. Shear stress is not easily measured for pulsatile flows. The time-varying velocity and velocity gradient must be measured very close to a wall, which is technically difficult. The gradient will depend strongly on the accurate measurement of distance from the wall and the shape of the velocity profile. An alternative method is to use a shear stress sensor that measures the heat or mass transfer between two adjacent points on the wall. However, this sensor must be imbedded in the wall and the flow must be steady and unidirectional. Shear stress also depends on the viscosity of the fluid. For blood flow, the viscosity very near a wall is not precisely known. Thus arterial wall shear stress measurements are estimates and may have errors of 20–50%.

At the lumenal surface, shear stress can be sensed directly as a force on an endothelial cell. In contrast, flow rates cannot be directly sensed by cells. To do so, an endothelial cell would require information on blood velocities far away from cells in the artery wall as well as the ability to integrate the velocities to give the volume flow rate. Thus, it is physically more natural for endothelial cells to sense and respond to shear stress than flow rate.

Arteries typically adapt to maintain a wall shear stress of approximately 15 dynes cm^{-2} (Glagov et al 1988). This value appears to be the same for different arteries within individual animals and for arteries from different animal species. Moreover, single arteries adapt to large changes in flow in order to

maintain this stress value. The blood-wall shear stress modulates diameter adaptive responses, intimal thickening, and platelet thrombosis. The wall shear stress is thus central to the vascular response to hemodynamics.

Hoop Stress

The other major hemodynamic force on an artery is the transmural pressure across the thickness of the wall. Arteries have a mean pressure of approximately 100 mm Hg, whereas veins have pressures of approximately 10 mm Hg. The blood pressure distends the vessel like a balloon, so the vessel must resist this distention force with a hoop stress in the circumferential direction. The hoop stress can be estimated by Laplace's Law as

$$\sigma = \frac{PR}{t}$$

(where R is the radius and t is wall thickness) for vessels with circular lumens that are not too thick (Fung 1984). Elaborate biomechanical models and measurements must be made to determine in detail levels of stress within diseased vessel walls. However, most normal healthy arteries yield an average hoop stress of approximately 10^5 Pa. This value again appears to hold over a wide range of conditions in many animal species (Glagov et al 1988). Whereas shear stress typically affects endothelial cells, hoop stress typically affects the smooth muscle cells in the tunica media. The hoop stress is the primary force in regulating wall thickness and residual stress in response to blood pressure and hypertension (Liu & Fung 1993). Pulsatile pressure induces the artery to pulsate or stretch with each cardiac cycle. The stretch may be easily sensed by the tunica media and smooth muscle cells that populate this layer. In the laboratory, hoop stress is hard to measure, whereas circumferential strain is rather easily measured. The primary determinant of the smooth muscle cell (SMC) response may be the local strain of these cells. This strain can be static, as with an isotonic load, or cyclical. The arterial wall may remodel itself in response to both static and cyclical loading conditions through secretion and organization of collagen and elastin, respectively (Rodbard 1970).

FLOWS IN SPECIFIC ARTERIES

Four parts of the arterial tree can serve as prototypic examples of hemodynamics: the heart and proximal aorta, the abdominal aorta, the carotid bifurcation, and the left coronary artery. These vessels exhibit flow characteristics seen in most of the arterial tree and are important because they often become diseased.

Flows in the heart and great vessels are dominated by inertial forces rather than viscous forces. Reynolds numbers at peak systole are on the order of

4000. The flow in the aorta and pulmonary trunk is similar to an entrance-type flow that is not developed. Consequently, the core of the flow can be considered an inviscid region that is surrounded by a developing boundary layer at the wall. The pressure and velocity patterns in a complex chamber of the heart can be modeled in three dimensions, including a moving boundary condition that develops tension (Peskin & McQueen 1989, Yoganathan et al 1994). Alternatively, in vitro models of the heart and great vessel anatomy can be studied in the laboratory. Flow can now be measured directly in the human heart using techniques such as catheters, Doppler ultrasound, and magnetic resonance velocimetry. These studies show that a large secondary flow in the ventricle is produced by inflow from the atrium through the mitral valve. The secondary flow can persist throughout diastole until the ejection phase. Systolic ejection is similar to a bellows-type flow with lateral pressure creating axial flow out of the aortic valve. In the ascending arch, potential flow theory predicts a skewing of the velocity profile toward the inner wall of the bend. Pressure differences caused by the velocity distributions can account for valve motion and closure (Fung 1984).

The abdominal aorta is the large vessel from the heart that traverses the middle of the abdomen and bifurcates into two arteries supplying the legs with blood. On the upstream end, flow comes from a relatively straight descending thoracic aorta and immediately branches laterally into two renal arteries and anteriorly into the celiac trunk at the level of the diaphragm. The renal arteries have a low resistance so that two thirds of the entering flow leaves the abdominal aorta through these three branches at the diaphragm. During rest conditions, the leg muscle requires little blood flow and has a high resistance. Only one third of the thoracic aorta flow passes into the legs through the abdominal aorta. Curiously, atherosclerotic disease extends along the posterior wall of the relatively straight abdominal aorta downstream of the renal arteries in all people. Little disease is present in the upstream thoracic aorta.

A typical Reynolds number for the abdominal aorta is 600 at rest, but it may increase 10-fold with exercise conditions. The Womersley parameter is about 16 and the lumbar curvature has an approximate Dean number of 260. Thus one would expect a rather blunt set of velocity profiles and limited amount of velocity skewing. Experimental visualization of flow in glass tube models of the abdominal aorta demonstrates the importance of three factors: (*a*) the branching flows at the diaphragm, which create several strong vortices just downstream of the renal arteries, (*b*) the lumbar curvature, which skews the flow toward the anterior wall of the abdominal aorta, and (*c*) the low distal impedance in the renals, which creates a suction effect that causes blood at the posterior wall of the aorta to reverse and flow back upstream into the renal arteries (Moore et al 1992). The net result is that the velocity profiles are

somewhat blunt as predicted (shown in Figure 5), but the outflow conditions combine with curvature to create an oscillation in velocity direction near the wall of the aorta, with a corresponding low average wall shear stress. The area of low and oscillatory wall shear stress correlates very well with the location of atherosclerotic plaque measured in autopsy specimens, $p < 0.001$ (Friedman et al 1986, Moore et al 1994c). As verification, measurements of in vivo flow in humans exhibit the same skewing and time-varying velocity profiles as produced in the glass-blown aortic model (Moore et al 1994b).

The carotid artery bifurcations are located along the sides of the neck. These arteries supply the brain and face with blood. Atherosclerosis, which develops right at the bifurcation, causes the majority of strokes in patients. A unique feature of the branch is an anatomic sinus, or expansion at the origin of the internal carotid artery. Figure 4 shows hydrogen bubble visualization of flow at the carotid bifurcation. The main stream moves upward along the centerline and flow divider along the posterior wall. In addition, counter-rotating secondary vortices move upstream toward the common carotid in a separation region. The mean Reynolds number is approximately 300, and the Womersley parameter is about 4. The daughter branches are about 25° off axis of the parent artery, on average. From the basic nondimensional scales, one would predict a series of parabolic profiles at this Womersley parameter value, with profile skewing and secondary flows generated by the branch, consistent with an analogous Dean number. A 1D, unsteady flow analysis of the sinus area enlargement suggests that an adverse pressure gradient may be present during the downstroke of systole and thus may induce flow separation (Giddens & Ku 1987). This analysis further suggests that flow separation should be transient because the pressure gradient is favorable during the upstroke of systole. Measurements of velocity have been made using laser Doppler anemometry (LDA) in machined plastic models of this bifurcation (Ku & Giddens 1987).

Secondary flows are indeed produced downstream of the bifurcation (Figure 4). Velocity profiles obtained through LDA and computational fluid dynamics (CFD) quantify the extent of reverse velocities near the outer wall of the internal carotid sinus (Figure 6). A region of transient flow separation is created along the posterior wall of the carotid sinus, which is prominent during the downstroke of systole. The artery wall in the sinus region would experience oscillations in near-wall velocity and a low mean wall shear stress. Atherosclerotic plaque is highly localized to a small area within this sinus region and correlates with low and oscillatory wall shear stress with coefficients greater than 0.9, $p < 0.001$. Comparison of the unsteady, 3D in vitro results with in vivo measurements obtained using Doppler ultrasound confirms that the assumptions of the laboratory model are valid (Ku et al 1985a). Several groups have recently used computational fluid dynamics to study the effects of wall elasticity and

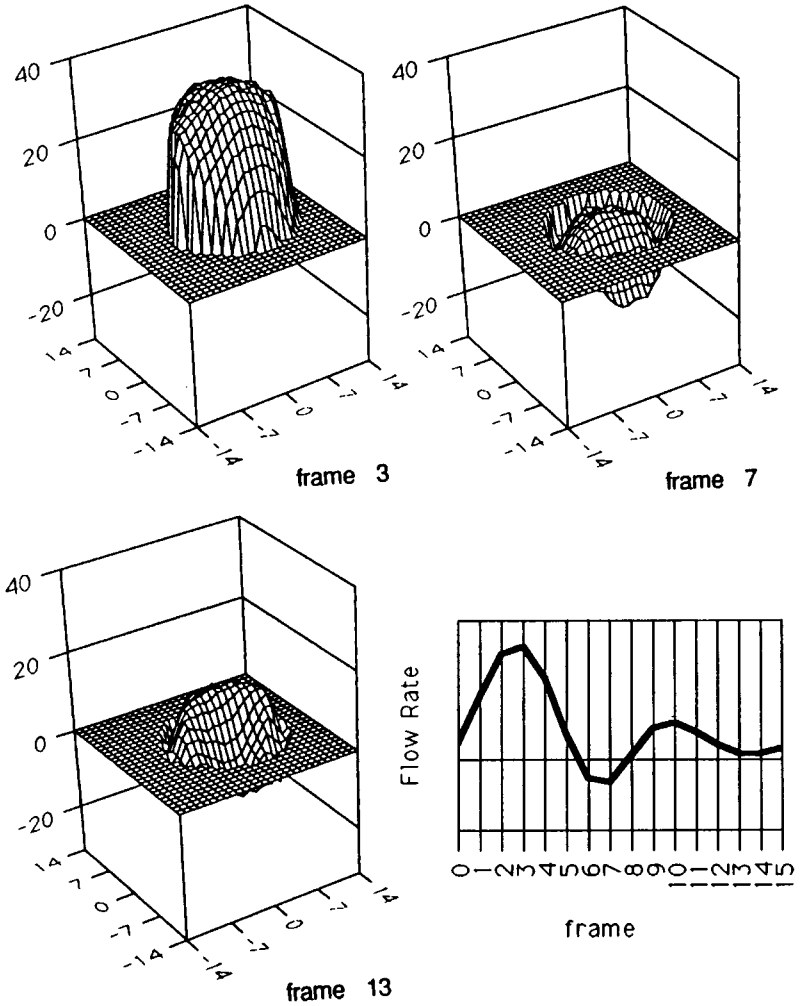

Figure 5 Velocity profiles in the abdominal aorta as measured with magnetic resonance velocimetry. Flow is positive during systole (frame 3). In frame 7, velocity at the walls reverses strongly and persists in the negative direction at the posterior wall at the end of diastole (frame 13). (Reprinted with permission of R. G. Landes Company.)

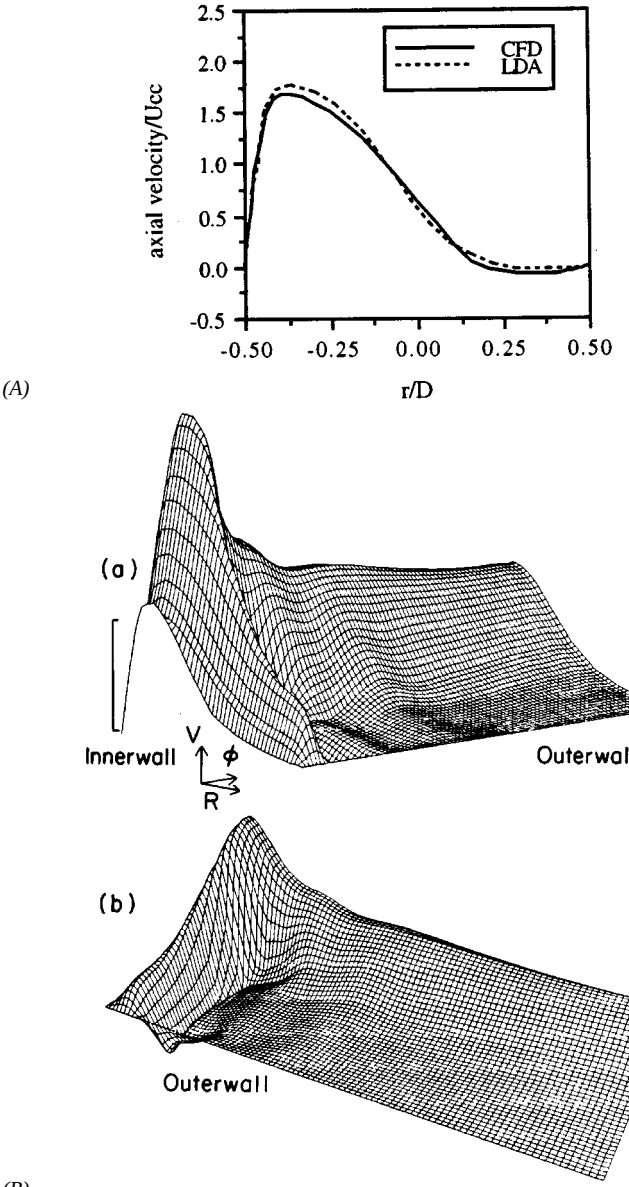

Figure 6 (*A*) Axial velocity profiles in the sinus region of a 3D model of the carotid bifurcation using laser Doppler anemometry and computational fluid dynamics. (*B*) Flow in the carotid sinus is unsteady with a transient reverse flow at the outer wall shown in this 3D plot of velocity vs diameter position and time. (Reprinted from Ku & Giddens, *Journal of Biomechanics* 20:407–421, 1987; reprinted with kind permission from Elsevier Science, Ltd, The Boulevard, Langford Lane, Kidlington OX5 IGB, UK.)

non-Newtonian viscosity (Reuderink 1991, Anayiotos 1994, Perktold et al 1991). These effects are small compared with the anatomic and flow variations between patients (Perktold & Rappitch 1995).

Flow at the left coronary artery bifurcation is complicated by several features (Bargeron et al 1988). First, the left main coronary artery is quite short, leading to an entrance type flow at a low Womersley parameter of 3. Second, the flow pattern in the left coronary artery is reversed compared with that of most arteries—flow is greater during artery diastole. Moreover, flow can be reversed during systole. The high pressures in the myocardium during systolic contraction cause the blood flow to reverse direction in the coronary arteries. Third, the bifurcation does not lie in a single plane but curves around the heart while branching. These features make it difficult to predict the velocity field a priori because several competing factors are in balance. From the short left main, one may predict a pulsatile set of blunt velocity profiles.

The curvatures likely set up secondary flows during part of the cardiac cycle. The coronary fluid dynamics have been studied using large-scale experimental models (Tang 1990) and spectral element computational modeling (He & Ku 1996). The left main coronary artery flow is similar to a piston flow with flat velocity profiles. As with all arterial branches, the velocity profiles are strongly skewed at the flow divider. Figure 7 illustrates two velocity profiles at two time points during the cardiac cycle that illustrate a strong reverse wall shear stress at the corners opposite the flow divider. A complex set of interacting vortices is produced in each branch from the compound curvatures. The secondary flows do not become pronounced until several diameters downstream of the bifurcation. The low momentum of fluid at the outer walls of the bifurcation causes fluid to oscillate in direction during the cardiac cycle. Comparison of the flow field with maps of atherosclerotic disease locations reveals a strong correlation between the inverse of mean wall shear stress and frequency of plaque ($r > 0.95$, $p < 0.001$) (He & Ku 1996). Surprisingly, variations in the left coronary branch angle do not alter the overall flow field regimes in a dramatic way (He 1993). However, changes in the coronary flow waveform significantly affect the magnitudes of oscillation (He 1993).

The analysis of hemodynamics in this representative set of arteries enables one to develop a general understanding of the fluid mechanics in the normal cardiovascular system. Lumped parameter models are useful for understanding the relationship between pressure and flow waveforms. However, blood flows are dominated by unsteadiness, convective acceleration, and viscosity, which allow for few simplifications. For specific flow situations, one can predict the hemodynamic situation by recognizing the appropriate Reynolds number and Womersley parameter range. Experimental and computational modeling can

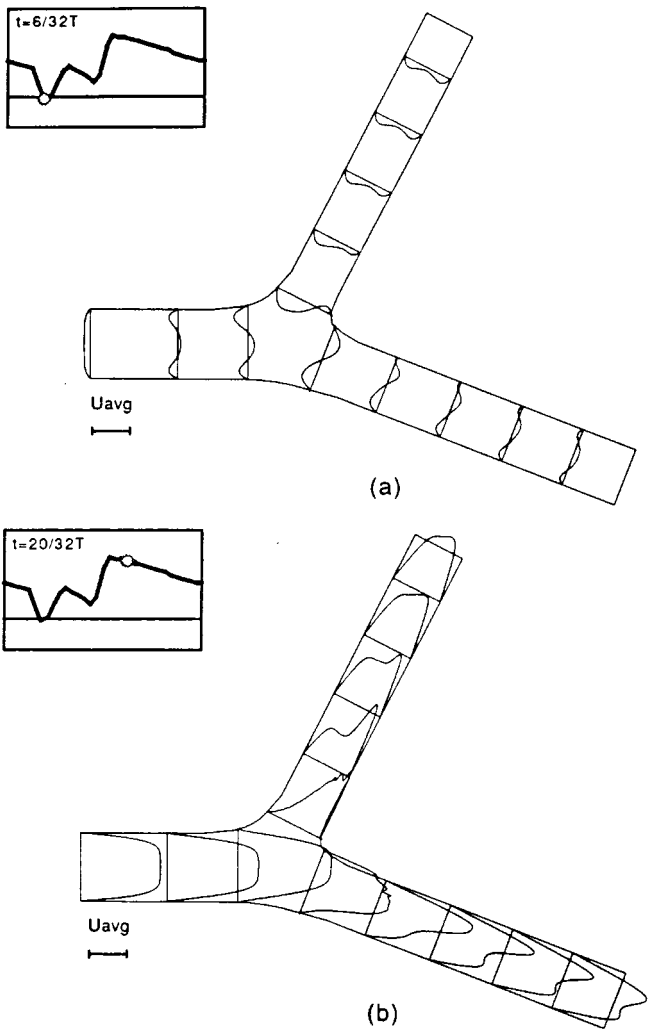

Figure 7 Representative velocity profiles in a model of the left coronary artery bifurcation as determined by a spectral element computational fluid dynamics simulation. (*a*) The profiles during systole show no flow reversal at the flow divider. (*b*) During diastole, the velocity profile is skewed toward the flow divider and develops a stair-step shape from the secondary flows. (From *Journal of Biomechanical Engineering*, 18:74–82; reprinted with permission of The American Society of Mechanical Engineers.)

then be used to quantify the local velocity distribution and wall shear stresses at important sites such as those prone to atherosclerotic disease. Luckily, elasticity and non-Newtonian viscosity are usually secondary factors that can be neglected. However, variations in branch anatomy and in pulsatile flow waveform and distribution can be expected to have significant effects. Arteries are not fixed tubes; they are biological organs that remodel themselves over time in response to hemodynamic stress.

BIOLOGICAL RESPONSES TO HEMODYNAMICS

The artery reacts to the dynamic changes in mechanical stress. Several physiologic responses are essential to maintain normal functioning of the circulatory system. The responses of arteries to the hemodynamic environment may constitute normal adaptation or pathological disease.

Hemostasis

Hemostasis is the arrest of bleeding. Trauma is a common occurrence, and the body must be able to deal with it. Therefore, hemostasis must occur on a very short time scale of milliseconds to minutes. When an artery is injured through trauma, blood quickly squirts out through the hole. The high outflow results in high shear stress, leaving collagen and tissue factor exposed. In this hemodynamic environment, hemostasis is initiated primarily through platelet activation and adherence. Platelet adhesion is modulated as much by shear rates as by such biological factors as density of Glycoprotein Ib (GPIb) receptors, von Willebrand factor (vWF) concentration, and exposed collagen (Hellums 1993, Markou et al 1993). For higher shear rates, platelet deposition can increase 100-fold, as illustrated in Figure 8 (Badimon et al 1986, Markou et al 1993, Fernandez-Ortiz et al 1994). Recent studies indicate that platelet-to-platelet aggregation may also be shear dependent. Conversely, when blood is stagnant, it will be clotted by a cascade of coagulation proteins. Coagulation is affected by the length of time blood is exposed to very low shear stress. Under this condition, thrombosis, or clotting of blood, is strongly modulated by the change in hemodynamic conditions that stimulates hemostasis (Hubbell & McIntire 1986). More study on hemostasis is needed before the effects of local hemodynamics can be fully understood.

Dilation and Contraction

On a longer time scale, an artery can respond to minute-to-minute changes in hemodynamics. The blood vessels must adapt to differing physiologic demands and conditions as blood pressure and flow change. Systemic flow adaptation can occur via several mechanisms, such as control of the heart rate and contractility by baroreceptors, flow distribution by local arteriolar autoregulation,

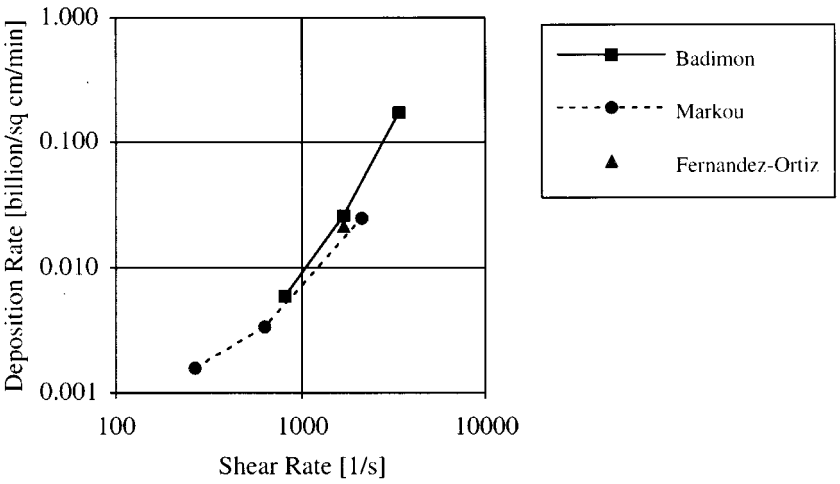

Figure 8 Platelet deposition rate vs wall shear rate for three different experimental preparations. Note that deposition rates are far in excess of a baseline rate of 105 in control arteries at normal shear rates.

and blood volume control by the kidneys. At a local level, arteries will dilate in response to increases in flow through an endothelial-dependent release of nitrous oxide (Furchgott 1993). The hemodynamic parameter governing this release is probably wall shear stress because total flow rate is not easily sensed. Blood vessels quickly contract in response to neurogenic or hormonal stimulation. Contraction is typically governed by the need to control systemic vascular resistance, venous pooling, and intravascular blood volume.

Adaption and Remodeling

Arteries adapt to long-term increases or decreases in wall shear stress. The response to increased wall shear stress is to vasodilate and then remodel to a larger diameter with the same arterial structure. This adaptation is commonly seen after the creation of an arterio-venous fistula for hemodialysis access. Conversely, decreased flow rates will cause the intimal layer to thicken to reestablish a normal wall shear stress (Glagov et al 1988). Eventually, the artery may maintain a thickened intima or remodel to a normal artery of smaller diameter.

On an even longer time scale of weeks to months, arteries will remodel their intima and media layers. The medial thickness is influenced by the local amount of hoop stress and nutrition. The tunica media is composed of lamellar units, each of which can bear a certain amount of hoop stress (Clark & Glagov 1985).

As described above, hoop stress increases with blood pressure. The media thickens through the addition of lamellar units until the total load can be borne comfortably by each lamellar unit. As the formation of a lamellar unit requires the proliferation of smooth muscle cells and the creation of a highly organized extracellular structure, the process may take several days. Alterations in the pulsatile pressure lead to changes in the organization of the elastin and collagen structure within the media (Rodbard 1970, Glagov et al 1988).

Several groups have studied the effects of flow, shear stress, and stretch on arteries in vivo. Flow can be augmented through an artery by an arterio-venous fistula. Increased flow causes the artery to dilate until the wall shear stress reaches the baseline level of the artery (Kamiya & Togawa 1980, Zarins et al 1987). Restricted flow through an artery produces a smaller-diameter vessel. A baseline appears to be approximately 15 to 20 dynes cm^{-2} for most arteries in a wide range of species (Glagov et al 1988).

Pathology

Several pathological states may arise from an excessive or uncontrolled response to a hemodynamic stimulus. Long-term hypertension produces a generalized medial thickening of blood vessels. Pulmonary and systemic hypertension will create stiff, thick arteries that can restrict blood flow and do not respond to the normal physiologic fluctuations in blood flow. Veins placed in the arterial system as vascular grafts develop a medial thickening that can create stenoses. Vascular grafts that are small in diameter tend to occlude rapidly. One contributing factor may be the very high shear stresses created in this situation, because wall shear stress increases to the third power as the diameter changes. Such high shear conditions may overstimulate platelet thrombosis, causing a total occlusion (Folts et al 1976).

Vascular grafts that are too large in diameter may stimulate a different response. In this case, wall shear stress will be abnormally low, and intimal thickening may be stimulated. Studies of intimal hyperplasia in a canine model indicate that low shear stresses can induce an accelerated amount of intimal thickening. Shear stress can also be varied in a single artery by inserting a tapered vascular graft with different diameters. In this case, intimal thickening results from low shear stresses even for a constant flow rate, as depicted in Figure 9*A* (Salam et al 1996).

Atherosclerosis forms over decades. This disease occurs in only a few places in the systemic vasculature, primarily the carotid artery sinus, the coronary arteries, the abdominal aorta, and the superficial femoral arteries. In localized sites of each of these arteries, the mean wall shear stress is very low and oscillates between positive and negative directions during the cardiac cycle. Comparison of the sites of disease with the local hemodynamic conditions reveals a consistent

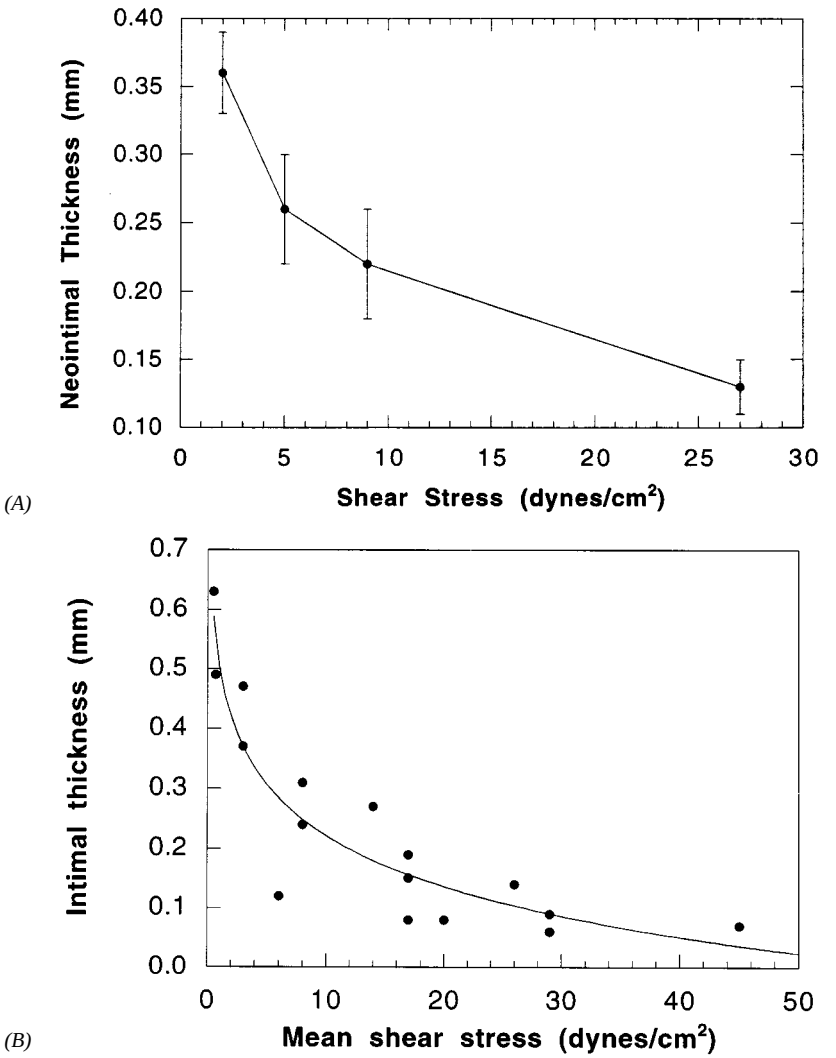

Figure 9 (*A*) Neointimal hyperplasia thickening vs wall shear stress in a dog arterial graft. The inverse relationship indicates more thickening at low shear stresses. (*B*) Atherosclerotic intimal thickening vs wall shear stress in human carotid arteries. The reciprocal relationship holds for mean and maximum wall shear stresses and correlates directly with oscillatory shear stress.

curve in which low wall shear stress is strongly correlated with atherosclerotic intimal thickening (Figure 9*B*) (Ku et al 1985b, Moore et al 1994b, He & Ku 1996). Most intimal thickening occurs where the average wall shear stress is less than 10 dynes cm^{-2}, and the pattern follows the inverse relationship shown for intimal hyperplasia and arterial adaptation. Thus the biological pattern of arterial response to shear stress appears to be preprogrammed.

In a field of cellular and tissue engineering currently under development, cultured cells and tissues are subjected to well-defined stresses in an in vitro environment. The creation of flow chambers that recreate physiologically realistic in vivo stresses is an important area of research (Helmlinger et al 1991, McIntire 1994, Moore et al 1994c).

The effects of hemodynamics on convective mass transfer should not be neglected. Most biologically active molecules are convected from one site to another. These molecules may be nutrients, wastes, growth factors, or vasoactive compounds. Systemic hormones reach an artery by convection and then may diffuse through the wall. In this situation, the intima is a major barrier. However, convective mass transport may be a limiting factor for small molecules such as nitrous oxide and oxygen, which diffuse rapidly through the wall. Such convection would be impaired in areas of flow separation or reversing wall shear at sites prone to atherosclerosis. Alternatively, biologically active molecules released by endothelial cells may have an effect downstream if the molecules are trapped in a boundary layer near the wall. The entrapment of molecules in this boundary layer can be used to deliver a high concentration of drug or antibody to the arterial wall (Chen et al 1995). Knowledge of the local hemodynamic conditions in these situations is essential for the prediction of a local biological effect that may not occur systematically.

HEMODYNAMICS OF STENOSES

When arteries become severely diseased, the arterial lumen becomes locally restricted over a 1-cm distance. This constriction is commonly referred to, clinically, as a *stenosis*. Figure 10, an X-ray angiogram of an atherosclerotic carotid artery, shows an example. The shape of a stenosis is similar to that of venturi, flow nozzle, or orifice. Hydrodynamic studies of these flow constrictors can directly provide such information as measurements of pressure drop vena contracta and nonrecoverable head loss due to separation and turbulence. In clinical medicine, stenoses are commonly defined as percent occlusion by diameter:

$$\text{Percent stenosis} = \frac{D_1 - D_2}{D_1} \times 100\%.$$

As disease advances, so does the percent stenosis. Note that continuity is usually written as a function of area ($Q = V \times A$), and some papers define a

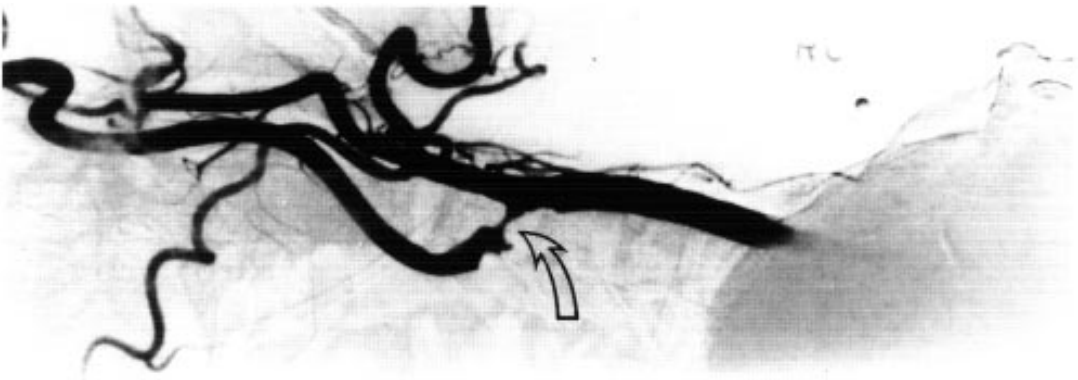

Figure 10 X-ray contrast angiogram of a diseased carotid bifurcation illustrating the focal nature of a stenosis. This stenosis will reduce blood flow and pressure to the brain. (From Strandness & van Breda, eds. 1994. Vascular Diseases: Surgical and Interventional Therapy. Reprinted with permission of Churchill Livingstone Inc.)

percent stenosis by area. Most physicians refer to a diameter reduction, and care should be used in translating results. Velocity through the throat does not rise as a linear function of percent diameter stenosis, but as the square. Head loss will also be a nonlinear function of stenosis. Pressure losses generally become significant only for stenoses greater than 50–75% (e.g. Young 1979) and depend on orifice shape and upstream Reynolds number. Thus one must account for these differences when attempting to predict pressure losses based on flow rate or velocity measurements in stenoses (Oshinski et al 1995b).

Stenotic flows have been well characterized in several studies. In sum, flow separation occurs in the expansion region at Reynolds numbers on the order of 10 for a 70% stenosis; a strong shear layer develops between the central jet and the recirculation region; the critical upstream Reynolds number for turbulence is approximately 300; turbulence intensity levels reach up to 100% of the upstream velocity values; and the turbulence is high for approximately 1.5 to 6.0 diameters downstream (Young 1979, Lieber & Giddens 1990). Figure 11 shows an example of turbulence at three levels of arterial stenosis (Khalifa & Giddens 1981). Pulsatility creates a periodic generation of turbulence, which is greatest during the deceleration of systole and least during the upstroke of systole. Both time and frequency domain analyses have been used to study the different characteristics of this transition to turbulence. A reduced wall shear stress has been calculated for numerous nonturbulent flows through stenoses (Siegel et al 1994).

For stenoses greater than 75%, several mechanisms severely limit flow. Turbulence downstream of the stenosis is very large and creates significant

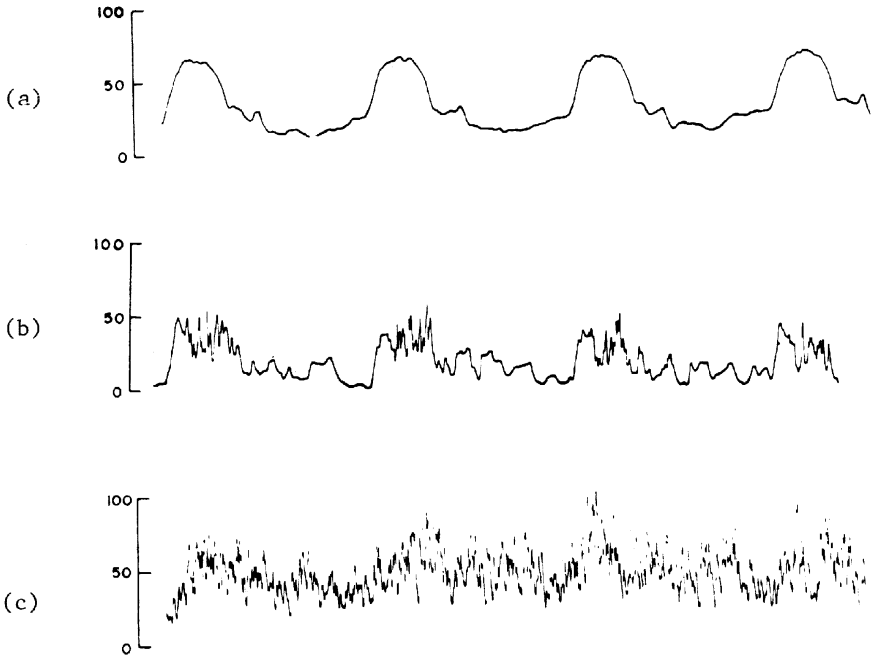

Figure 11 Velocity waveforms, obtained with a hot-film anemometer, distal to aortic stenoses in the descending thoracic aorta of a dog. Disturbances are not present in the 0% stenosis but are present during the deceleration phase of systole in the 33% stenosis and throughout the cycle in the 66% stenosis. Note the loss of pulsatility with higher grades of stenosis. (From Khalifa & Giddens, *Journal of Biomechanics* 11:129–141, 1978; reprinted with kind permission from Elsevier Science Ltd, The Boulevard, Langford Lane, Kidlington OX5 IGB, UK.)

resistance. The critical Reynolds number for turbulence rapidly falls for stenoses greater than 25%. At 50% stenosis, turbulence is generated throughout the pulsatile cycle (Khalifa & Giddens 1981). At higher levels of stenosis, turbulence is severe and accounts for about 80% of the pressure loss.

Separation of flow can also contribute to pressure loss and is a major factor at lower percent stenoses. For a moderate level of stenosis, the critical Reynolds number for separation is only 10. Thus separation will occur in most arterial stenoses. A strong shear layer at the interface of the separation region and the central jet creates additional viscous losses. The throat of the stenosis is a site of high shear rates at the wall, which also contribute to viscous losses. For low-grade stenoses, the wall and separation shear layers produce most of the losses. For high-grade stenoses, turbulence is the major loss mechanism (Ku et al 1987).

Collapsible Stenoses

Collapsible tube theory presents another mechanism for flow limitation. Blood flow through the constricted area of a severe stenosis is similar to that through a venturi or flow nozzle. In the contraction section, the blood can accelerate to high speeds of over 6 m s^{-1}. In this situation, the external pressure may be greater than the internal fluid pressure, and the artery could collapse. Because in most arteries flow is greater during systole, collapse would likely occur during this period. Flow in compliant collapsible tubes can be choked similar to the way compressible flow is choked in a laval nozzle. Choking acts like an additional resistor and also limits the flow for arterial stenoses in the range of 80–90%.

Shapiro (1977) has elegantly described the basic fluid dynamics of collapsible tubes. He drew the analogy between collapsible tube flow and compressible and open-channel flows. The 1D Euler equation is identical for these three flows. Continuity is governed by

$$\frac{\partial A}{\partial t} + \frac{\partial}{\partial x}(Au) = 0$$

for a collapsible tube, where $A(t, x)$ is the cross-sectional area,

$$\frac{\partial \rho}{\partial t} + \frac{\partial}{\partial x}(\rho u) = 0$$

for compressible flow with density ρ, and

$$\frac{\partial h}{\partial t} + \frac{\partial}{\partial x}(hu) = 0$$

for open-channel flow with height h.

For the collapsible tube, the area is a function of time and axial position. Along with these two equations, an equation of state must be given to solve for the three unknowns of pressure, velocity, and area. For elastic tubes, this pressure-area relationship is called the tube law. Analysis of this flow can be approached using mathematical modeling or through experimentation.

A crucial bit of information required for the solution is the tube law of an artery for both positive and negative transmural pressures. Measurements of the pressure-diameter relationship for arteries yield a complex relationship shown in Figure 12 (Powell 1991). The plot for positive pressures exhibits a nonlinear strain-stiffening behavior well known for biological materials. A simple relationship of the tube law that models this general behavior has been proposed by Elad and colleagues (Elad et al 1987, Elad & Kamm 1989) for the entire range of positive and negative pressures:

$$P = A^{n_1} - A^{-n_2},$$

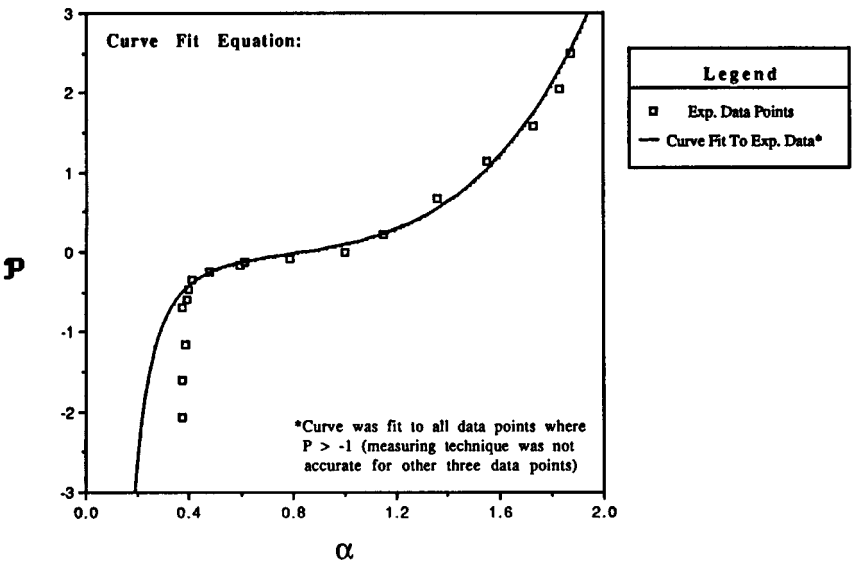

Figure 12 Tube law relating pressure and area for a bovine artery over positive and negative transmural pressures. The curve exhibits low stiffness at small negative pressures associated with collapse. The tube wavespeed will be proportional to the stiffness, which is indicative of low wavespeeds at collapse. The fitted curve is of the form $P = A^{n_1} - A^{-n_2}$.

where P is a nondimensional pressure and A is a nondimensional area. At negative pressures, the modulus of elasticity becomes very small as the tube collapses on itself. At strongly negative pressures, the collapsed tube is fairly stiff because the opposing walls are in contact. The solid mechanics of the collapse of thick arteries with an eccentric plaque has also been analyzed and qualitatively exhibit a similar behavior (Aoki & Ku 1993). This relationship shows that small changes in pressure induce large changes in area in tubes that collapse. Ultimately, the tube can be used to approximate a local elastic tube pressure wavespeed using

$$c^2 = \frac{A}{\rho}\frac{\partial \rho}{\partial A}.$$

The solution for the governing equations is well-known and exhibits a key feature of transition from subcritical flows to supercritical flows (Shapiro 1977). When the tube begins to collapse, it is very floppy, and the local wavespeed falls to about one tenth the value in the distended tube. The local fluid velocity can reach the same value as the local tube wavespeed. This ratio of local velocity to local tube wavespeed is given as:

$$S = u/c,$$

which Shapiro termed the speed index and is analogous to a Mach or Froude number. For subcritical flows, the speed index S is less than 1; a value $S > 1$ indicates a supercritical flow. In addition, a transition from supercritical to subcritical flow can occur through an elastic jump analogous to a sonic shock, and maximum flow passes through the tube when its throat is at the critical condition, called *choking*. The analogy is not perfect for higher dimensions because the density is a property of the fluid, and gravity acts as a body force on every element of the fluid, whereas the area changes are actually boundary conditions on the flow.

Because the equations retain the convective nonlinear term, a numerical iterative solution can be obtained (Ku et al 1990b). Figure 13*a* shows the area variation along the length of the stenosis during flow in comparison with the nominal distended area (no flow). This model demonstrates the acceleration of velocity in the convergent section with a corresponding decrease in the wavespeed through the throat, as shown in Figure 13*b*. Collapse occurs at the throat and extends for about 0.3 diameters downstream, where an elastic jump restores the tube to a distended area. The model can be used to evaluate the importance of various factors by studying a range of parameters. The critical flow rate for collapse depends most strongly on percent stenosis. Frictional losses and the stiffness of the tube near the throat weakly affect the critical flow rate (Downing & Ku 1993).

The collapsing flow through these stenoses can be demonstrated experimentally using either an orifice-type stenosis or a smoothly tapered hourglass configuration. One can experimentally determine a critical flow rate for collapse and choking for a given percent stenosis (Biz et al 1993). Stenosis severity remains the dominant factor for collapse under physiologic conditions. Upstream pressure, stenosis stiffness, and axial strain are weak influences. When the stenosis begins to collapse, an unstable cycle is set up. As the collapse increases, the resistance to flow increases and the flow rate drops. The decreased flow reduces the throat velocity; the pressure increases; and the tube reopens. The velocity then accelerates and collapses the tube. An oscillation in wall motion is seen in silicone tubes, which have a rich set of complex modes (Moore et al 1995). Such unstable wall oscillations have been explored in depth by Cancelli & Pedley (1985) and Bertram et al (1989). Interestingly, oscillations and flow choking occur at the same critical flow rate, which makes them easy to discern in the laboratory.

Collapse of an artery also results from the measurement of blood pressure using an external cuff, a device known as a *sphygmomanometer*. When the cuff is inflated to pressures greater than the blood pressure, the artery will collapse. As the external pressure is reduced, the artery will reexpand during systole, producing a tapping sound. After systole, the artery will again collapse during

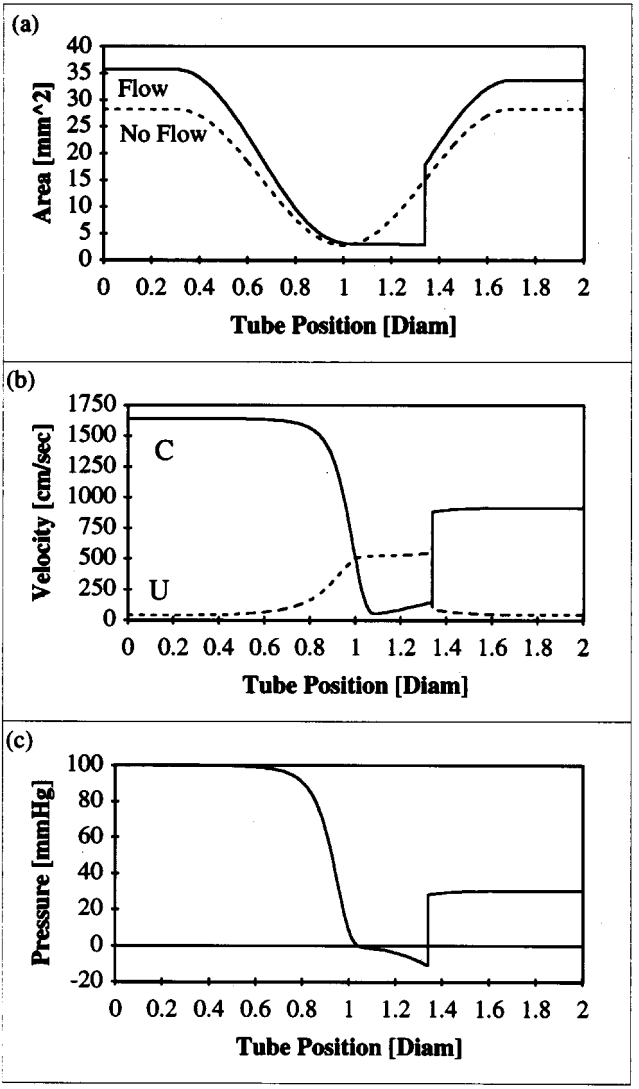

Figure 13 (*a*) Area, (*b*) velocity, and (*c*) pressure distribution along the length of an elastic stenosis with flow. Tube collapse occurs when the velocity equals the wavespeed at tube position 1.00. Tube re-expands at the elastic jump from supercritical flow to subcritical flow at tube position 1.35.

diastole. Other examples of physiologic flow through collapsible tubes are the trachea, which can collapse during coughing, and veins when the blood is at low pressure.

Two important clinical consequences arise from the collapse of stenoses. First, choking reduces the flow rate beyond the losses associated with turbulence alone. This flow limitation, or critical flow rate, has long been observed by physiologists and described as the coronary flow reserve. Even with decreases in distal resistance, the critical flow rate is very small. Estimates of coronary flow reserve should include this choking flow limitation as well as other forms of viscous losses (Gould 1978, Santamore et al 1982).

A second consequence is the loading conditions imposed on an atherosclerotic plaque. Arteries are well built as pressure vessels for tensile stress. The microarchitecture consists of a reinforced composite tube with collagen and elastin fibers running in the circumferential direction. Stenotic flow collapse creates a compressive stress that may buckle the fibers. Mechanical experience with composite structures indicates that these materials are quite strong in the tensile direction of the reinforcing fibers, but they break down rapidly under compression, especially cyclic compression, when cracks and delaminations develop. The oscillations in compressive loading may induce a fracture fatigue in the surface of the atheroma, causing a rupture of the plaque cap. Plaque cap rupture is the precipitating event in most heart attacks and strokes, and the mechanical interactions between fluids and solids that occur in high-grade stenosis may contribute to the catastrophic material failure (Ku & McCord 1993).

Diagnosis of Disease

Hemodynamic studies of stenoses have many clinical applications. One area of investigation revolves around the diagnosis of severe stenosis. The most accepted clinical predictors of impending heart attack, stroke, and lower-limb ischemia are based on the presence of hemodynamically significant stenoses. The arts of cardiology and vascular surgery change constantly, but current treatments for cardiovascular disease are based on the severity and location of stenoses. For carotid artery disease, surgery is recommended to patients with stenoses greater than 75% (NASCET 1991). For coronary artery disease, the type of treatment is often based on whether the coronary artery is more than 75% stenotic; in the left main coronary artery, the percentage is 50% (Chaitman et al 1981). Currently, the best indicator for surgical treatment of arteriosclerosis is the degree of stenosis. One can determine the anatomy of the lesion using X-ray contrast angiography. This technique yields a percent stenosis but says little about the flow rate, flow reserve, or nature of the plaque. Although X-ray angiography is currently the standard diagnostic procedure, cost and morbidity are distinct disadvantages.

The severity of the stenosis may be indirectly obtained from the fluid mechanics of stenoses. For example, one can use Doppler ultrasound to measure the increased velocities in the stenotic jet and back out a percent stenosis (Figure 14) (Dawson & Strandness 1994). This technique is widely used to determine levels of stenosis in carotid artery disease with an accuracy of 90%. Doppler ultrasound can also be used to measure the flow waveform in leg arteries. Normal arteries have a characteristic triphasic pattern, whereas diseased arteries with a stenosis exhibit a blunted monophasic pattern.

Stenoses will alter the pulsatile pressure waveforms by blocking higher frequencies and blunting the amplitude. A plethysmograph detects the local pulsatile volume changes in an extremity as a reflection of the local pressure waveform. Actual pressure traces can be obtained using an intravascular catheter connected to a high-fidelity pressure transducer.

Each of these clinical diagnostic tests has advantages and disadvantages for predicting hemodynamic significance. Standard angiography uses radiation, and an arterial injection can produce serious complications. Ultrasound studies have problems with aliasing, sample volume, transit time, and scattering (Garbini et al 1982). Furthermore, acoustic limitations of resolution and noise from scattering in deep tissue restrict the use of this technique to a few locations in the arterial tree. Plethysmography does not pinpoint the site of lesions. Intravascular pressure catheterization is invasive and difficult.

Recently, magnetic resonance imaging (MRI) has been proposed as a less expensive, less morbid alternative to X-ray angiography (Yucel 1994). In contrast to Doppler techniques, which require an acoustic or optical window, in MRI an electromagnetic window is used that does not interfere with the flow, so much more of the body can be studied. MRI would be a useful alternative to ultrasound, because resolution and depth are not critical limitations for this electro-magnetic probe. MRI is sensitive to the motion of protons and can be used to image moving blood by means of time-of-flight labeling or phase velocity mapping (PVM). These techniques are described more fully elsewhere (Yucel 1994). MR angiography is rather new, and the relationship between hemodynamics and signal detection is not completely understood (Siegel et al 1995). Hemodynamic studies using MRI indicate that signal is lost in the neighborhood of a stenosis. Signal levels decrease when flows become random or turbulent. Thus the strong turbulence in stenoses creates imaging signal loss (Oshinski et al 1995a). The relationship between turbulent fluid mechanics and MRI can be described mathematically, but the complexities of turbulence must be included in any interpretation of the images of stenoses. The signal blackout from stenosis is an important reason why MR angiography has not replaced conventional X-ray contrast angiography.

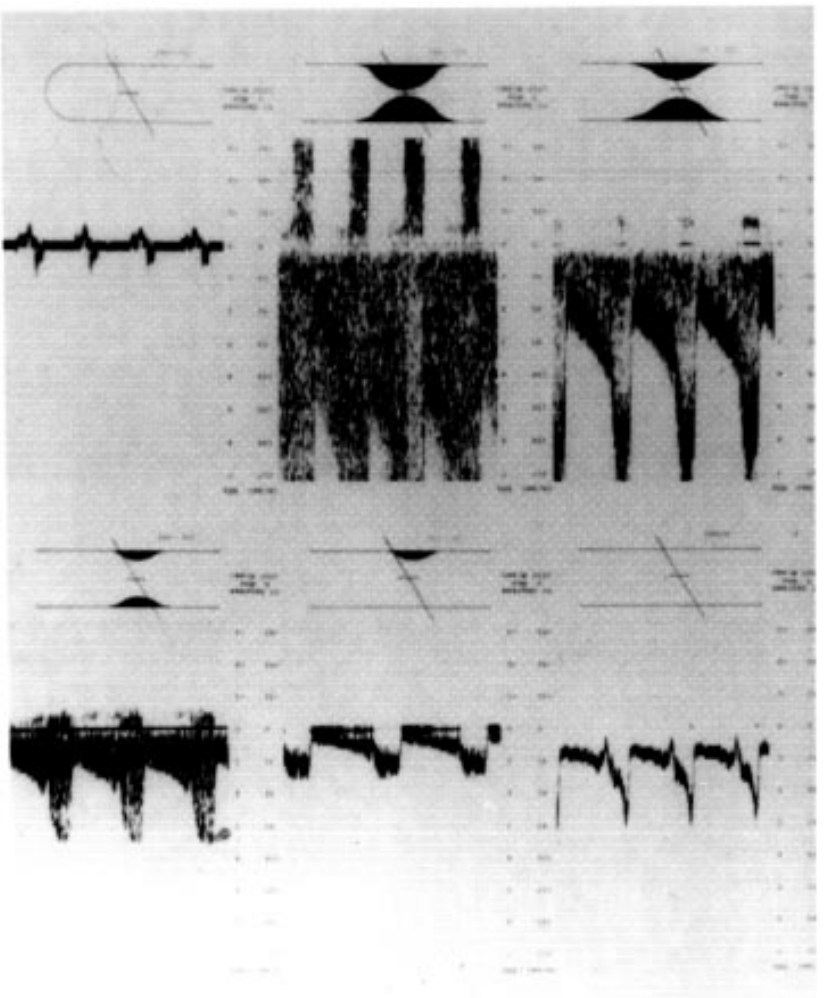

Figure 14 Duplex ultrasound characteristics at different levels of stenosis. The categories for percent stenosis are based primarily on the velocity values at the throat instead of the anatomic image. (From Strandness & Breda 1994; reprinted with permission of Churchill Livingstone, Inc.)

The measurement of velocity with MRI requires a constant velocity over the sample volume and time scale of the image acquisition. Stenotic flow violates this assumption. Velocity measurements are distorted in the presence of accelerations, such as in the convective acceleration region of a converging section or with temporal accelerations that result from turbulence. In the sections of the stenosis where the lumenal area changes, convective acceleration can introduce errors on the order of 50% (Oshinski et al 1992). In the region downstream of the throat, fluid motion is highly irregular and temporal accelerations from turbulence cause large errors in velocity measurement (Oshinski et al 1995a). Still, MR PVM retains some distinct advantages. PVM measurements are accurate for nonaccelerating flows, and the measurements require short data acquisition times. For example, velocity can be measured at 256×256 points across a test section in approximately 5 min, as illustrated in Figure 5.

Shear-Dependent Thrombosis

Stenotic flows are crucial to clinical disease in several other areas. After the plaque cap ruptures, the revealed contents of the atheroma stimulate a blood-clotting reaction called *thrombosis* (Fernandez-Ortiz et al 1994). For the arterial system, thrombosis is initiated by the adherence of platelets at the surface with rapid accumulation of additional platelets. In vitro experiments have produced conflicting results, but in vivo studies with nonanticoagulated blood indicate that platelets stick at the throat of the stenosis. The adherence and accumulation of these platelets are shear dependent with more accumulation at higher shear rates (Figure 7). The time scale of adhesion is on the order of milliseconds. Likewise, the adhesion strength must be enormous because the shear stresses on the platelet are large and increase as the throat clots up. An understanding of this phenomenon requires knowledge of molecular bioadhesion, two-phase slurry flows, convective mass transport, and the complicated events of thrombosis. In short, this subject will require intensive study for a long time before it is fully understood.

CONCLUSIONS

The study of the blood flow in arteries is a rich field encompassing unsteady flows, varying geometries, turbulence, and secondary structures. Arterial hemodynamics can be simplified as an unsteady internal flow. Specific arteries exhibit flow characteristics which are three-dimensional and developing. Diseased arteries can create high levels of turbulence, head loss, and a choked-flow condition in which tubes can collapse. The pulsatile nature of the flow creates a dynamic environment that raises many interesting and fundamental unsteady fluid mechanics questions. Answers to these questions can then be used to

predict and change blood flow to alter the course of disease. Each fluid mechanics aspect plays a role in the generation, detection, and treatment of arterial disease. Most of these diseases are highly focal and must be caused by a local factor acting at a specific site. Thus the focal hemodynamics must be characterized in detail at specific arteries. The quantities of stress and mass transfer at the blood-wall interface are important hemodynamic factors influencing biological responses.

The formation of a stenosis is the most dire biological response. Hence, complete understanding of the relationship between pressure, flow, and symptoms for cardiovascular stenoses remains a critical problem. New devices to repair stenotic arteries are now being developed. Cellular and tissue-engineered arteries will need bioreactor chambers that mimic the in vivo hemodynamic environment. Thus fluid mechanics will continue to play an important role in the future diagnosis, understanding, and treatment of cardiovascular diseases.

Literature Cited

Anayiotos AS, Jones SA, Giddens DP, Glagov S, Zarins CK. 1994. Shear stress at a compliant model of the human carotid bifurcation. *J. Biomech. Eng.* 116:98–106

Aoki T, Ku DN. 1993. Collapse of diseased arteries with eccentric cross section. *J. Biomech. Eng.* 26:2:133–42

Badimon L, Badimon JJ, Galvez A, Chesebro JH, Fuster V. 1986. Influence of arterial damage and wall shear rate on platelet deposition. Ex vivo study in a swine model. *Arteriosclerosis* 6:312

Bargeron CB, Deters OJ, Mark FF, Friedman MH. 1988. Effect of flow partition on wall shear in a cast of a human coronary artery. *Cardiovasc. Res.* 5:340–44

Bertram CD, Raymond CJ, Butcher KSA. 1989. Oscillations in a collapsed-tube analog of the brachial artery under a sphygmomanometer cuff. *J. Biomech. Eng.* 111:185–91

Biz S, Ku DN, Downing JM. 1993. Flow choking in elastic stenoses. Hemodynamic collapse of highly stenotic arteries. *Circ. Suppl.* 88(4):1363

Cancelli C, Pedley TJ. 1985. A separated flow model for collapsible tube oscillations. *J. Fluid Mech.* 157:375–404

Caro CG, Pedley TJ, Schroter RC, Seed WA. 1978. The Mechanics of the *Circulation.* New York: Oxford Medical

Chaitman BR, Fisher LD, Bourassa MG, Davis K, Rogers WJ, et al. 1981. Effect of coronary bypass surgery on survival patterns in subsets of patients with left main coronary artery disease. Report of Collaborative Study in Coronary Artery Surgery (CASS). *Am. J. Cardiol.* 48(4):765–77

Chen C, Hansen SR, Lumsden AB. 1995. Boundary layer infusion of heparin prevents thrombosis and reduces neointimal hypersia in venous polytetra fluoroethylene grafts without system anticoagulation. *J. Vasc. Surg.* 22:237–45

Chien S. 1970. Shear dependence of effective cell volume as a determinant of blood viscosity. *Science* 168:977

Clark JM, Glagov S. 1985. Transmural organization of the arterial wall: the lamellar unit revisited. *Arteriosclerosis* 5:19–24

Dean WR. 1928. The stream-line motion of fluid in a curved pipe. *Philos. Mag. Ser.* 7 5:675–95

Delfino A, Moore JE Jr, Meister JJ. 1994. Lateral deformation and movement effects on flow through dispensable tube models of blood vessels. *Biorheology* 31:533–54

Dawson DL, Strandness DE Jr. 1994. "Duplex scanning." In Strandness & van Breda, pp. 157–99

Downing JM, Ku DN. 1993. Flow through a compliant stenotic artery. *ASME Adv. Bioeng. BED* 26:137–40

Elad D, Kamm RD. 1989. Parametric evalua-

tion of forced expiration using a numerical model. *ASME J. Biomech. Eng.* 111:192–99

Elad D, Kamm RD, Shapiro AH. 1987. Choking phenomena in a lung-like model. *ASME J. Biomech. Eng.* 109:1–9

Eskey CJ, Wolmark N, McDonell CL, Domach MM, Jain RK. 1994. Residence time distributions of various tracers in tumors: implications for drug delivery and blood flow measurement. *J. Natl. Cancer Inst.* 86(4):293–99

Fernandez-Ortiz A, Badimon JJ, Falk E, Fuster V, Meyer B, et al. 1994. Characterization of the relative thrombogenicity of atherosclerotic plaque components: implications for consequences of plaque rupture. *JACC* 23(3):1562–69

Folts JD, Crowell EB, Rowe GG. 1976. Platelet occlusions. Platelet aggregation in partially obstructed vessels and its elimination with aspirin. *Circulation* 54: 365–70

Friedman MH, Bargeron CB, Hutchins GM, Mark FF, Deters OJ. 1980. Hemodynamic measurements in human arterial casts and their correlation with histology and luminal area. *J. Biomech. Eng.* 102:247

Friedman MH, Peters OJ, Bargeron CB. 1986. Shear-dependent thickening of the human arterial intima. *Atherosclerosis* 60:161–71

Fung YC. 1984. *Biodynamics: Circulation.* New York: Springer-Verlag

Furchgott RF. 1993. Introduction to EDRF research. *J. Cardiovasc. Pharmacol.* 22:51–52

Garbini JL, Forster FK, Jorgensen JE. 1982. Measurement of fluid turbulence based on pulsed ultrasound techniques. Part 2: Analysis. *J. Fluid Mech.* 118:445–70

Giddens DP, Ku DN. 1987. A note on the relationship between input flow waveform and wall shear rate in pulsatile, separating flows. *J. Biomech. Eng.* 109:175–76

Glagov S, Zarins C, Giddens DP, Ku DN. 1988. Hemodynamics and atherosclerosis: insights and perspectives gained from studies of human arteries. *Arch. Pathol. Lab. Med.* 112:1018–31

Gould KL. 1978. Pressure-flow characteristics of coronary stenoses in unsedated dogs at rest and during coronary vasodilation. *Circ. Res.* 43(2):242–53

He X. 1993. *Numerical simulations of blood flow in human coronary arteries.* PhD thesis. Georgia Institute of Technol., Atlanta

He X, Ku DN. 1994. Unsteady entrance flow development in a straight tube. *J. Biomech. Eng.* 116:355–60

He X, Ku DN. 1996. Pulsatile flow in the human left coronary artery bifurcation: average conditions. *J. Biomech. Eng.* 118:74–82

He X, Ku DN, Moore JE. 1993. Simple calculation of the velocity profiles for pulsatile flow in a blood vessel using Mathematica. *Ann. Biomed. Eng.* 21:45–49

Hellums JD, 1993. Whitaker lecture: biorheology in thrombosis research. *Ann. Biomed. Eng.* 1994 22:445–55

Helmlinger G, Geiger RV, Schreck S, Nerem RM. 1991. Effects of pulsatile flow on cultured vascular endothelial cell morphology. *J. Biomech. Eng.* 113:123–31

Holenstein R, Ku DN. 1988. Reverse flow in the major infrarenol vessels–a capacitive phenomenon. *Biorheology* 25:835–42

Hubbell JA, McIntire LV. 1986. Platelet active concentration profiles near growing thrombi–a mathematical consideration. *Biophys. J.* 50:937–45

Kamiya A, Togawa T. 1980. Adaptive regulation of wall shear stress to flow change in the canine carotid artery. *Am. J. Physiol.* 239:H14–21

Karino T, Goldsmith HL. 1979. Aggregation of human platelets in an annular vortex distal to a tubular expansion. *Microvasc. Res.* 17:217–37

Keynton RS, Rittgers SE, Shu MC. 1991. The effect of angle and flow rate upon hemodynamics in distal vascular graft anastomoses: an in vitro model study. *J. Biomech. Eng.* 113:458

Khalifa AMA, Giddens DP. 1981. Characterization and evolution of post stenotic flow disturbances. *J. Biomech.* 14:279–96

Kim WY, Walker PG, Pedersen EM, Poulsen JK, Oyre S, et al. 1995. Left ventricular blood flow patterns in normal subjects: a quantitative analysis by three-dimensional magnetic resonance velocity mapping. *J. Am. Coll. Cardiol.* 26:224–38

Ku DN, Biancheri CL, Pettigrew RI, Peifer JW, Markou CP, Engels H. 1990a. Evaluation of magnetic resonance velocimetry for steady flow. *J. Biomech. Eng.* 112:464–72

Ku DN, Giddens DP. 1987. Laser Doppler anemometer measurements of pulsatile flow in a model carotid bifurcation. *J. Biomech. Eng.* 20:407–21

Ku DN, Giddens DP. 1983. Pulsatile flow visualization in the carotid artery: arteriosclerosis. 3:31–39

Ku DN, Klafta JM, Gewertz BL, Zarins CK. 1987. The contribution of valves to sophenous vein graft resistance. *J. Vasc. Surg.* 6:274–79

Ku DN, McCord BN. 1993. Cyclic stress causes rupture of the atherosclerotic plaque cap. *Suppl. to Circulation* 88:(4:2):1362

Ku DN, Phillips DJ, Giddens DP, Strandness DE. 1985a. Hemodynamics of the normal human carotid bifurcation: in vitro and in vivo studies. *Ultrasound Med. Biol.* 11:13–26

Ku DN, Zarins CK, Giddens DP, Glagov S.

1985b. Pulsatile flow and atherosclerosis in the human carotid bifurcation: positive correlation between plaque localization and low and oscillating shear stress. *Arteriosclerosis* 5:292–302

Ku DN, Zeigler MN, Downing JM. 1990b. One-dimensional steady inviscid flow through a stenotic collapsible tube. *ASME J. Biomech. Eng.* 112:444–50

Lieber BB, Giddens DP. 1990. Post-stenotic core flow and its effects on wall shear stress. *J. Biomech.* 23(6):597–605

Liu SQ, Fung YC. 1989. Relationship between hypertension, hypertrophy, and opening angle of zero-stress state of arteries following aortic constriction. *J. Biomech. Eng.* 111(4):325–35

Markou CP, Hanson SR, Siegel JM, Ku DN. 1993. The role of high wall shear rate of thrombus formation in stenoses. *Adv. Bioeng. ASME BED* 26:555–58

McDonald DA. 1974. *Blood Flow in Arteries*. Baltimore: Williams & Wilkins

McIntire CV. 1994. Bioengineering and vascular biology. *Ann. Biomed. Eng.* 22:2–13

Meier D, Maier S, Boesiger P. 1988. Quantitative flow measurement on phantoms and on blood vessels with MR. *Magn. Reson. Med.* 8:25–34

Moore JE Jr, Burki E, Suciu A, Zhao S, Burnier M, et al. 1994a. Device for subjecting vascular endothelial cells to both fluid shear stress and circumferential cyclic stretch. *Ann. Biomed. Eng.* 22:416–22

Moore JE Jr, Ku DN, Zarins CK, Glagov S. 1992. Pulsatile flow visualization in the abdominal aorta under differing physiologic conditions: implications for increased susceptibility to atherosclerosis. *J. Biomech. Eng.* 114:391–97

Moore JE Jr, Maier SE, Ku DN, Boesiger P. 1994b. Hemodynamics in the abdominal aorta: a comparison of in vitro and in vivo measurements. *J. Appl. Physiol.* 76:1520–27

Moore JE Jr, Stergiopulos N, Golay X, Ku DN, Meister JJ. 1995. Flow measurements in a collapsible arterial stenosis model. *1995 Bioeng. Conf. ASME* 29:229–30

Moore JE Jr, Xu C, Glagov S, Zarins CK, Ku DN. 1994c. Fluid wall shear stress measurements in a model of the human abdominal aorta: oscillatory behavior and relationship to atherosclerosis. *Atherosclerosis* 110(2):225–40

Nerem RM, Seed WA. 1972. An in vivo study of aortic flow disturbances. *Cardiovasc. Res.* 6:1–14

Nichols WW, O'Rourke MF. 1990. *McDonald's Blood Flow in Arteries*. Philadelphia: Lea & Febiger. 3rd ed.

North American Symptomatic Carotid Endarterectomy Trial Collaborators (NASCET). 1991. Beneficial effect of carotid endarterectomy in symptomatic patients with high-grade carotid stenosis. *N. Engl. J. Med.* 325:445–53

Ohja M, Ethier CR, Johnston KW. 1990. Steady and pulsatile flow fields in an end-to-side arterial anastomosis model. *J. Vasc. Surg.* 12:747

Oshinski JN, Ku DN, Bohning DE, Pettigrew RI. 1992. Effects of acceleration on the accuracy of MR phase velocity measurements. *J. Magn. Reson. Imag.* 2:665–670

Oshinski JN, Ku DN, Pettigrew RI. 1995a. Turbulent fluctuation velocity: the most significant determinant of signal loss in stenotic vessels. *Magn. Reson. Med.* 33:193–99

Oshinski JN, Parks WJ, Markou CP, Bergman HL, Larson BE, et al. 1995b. Improved measurements of pressure gradients in aortic coarctations by magnetic resonance imaging. *ASME Proc. Bioeng. Conf.* 29:371–72

Pedley TJ. 1980. *The Fluid Mechanics of Large Blood Vessels*. Cambridge: Cambridge Univ. Press

Perktold K, Rappitch G. 1995. Computer simulation of local blood flow and vessel mechanics in a compliant carotid artery bifurcation model. *J. Biomech.* 28:845–56

Perktold K, Resch M, Florian H. 1991. Pulsatile non-Newtonian flow characteristics in a three-dimensional human carotid bifurcation model. *J. Biomech. Eng.* 13:464–75

Peskin CS, McQueen DM. 1989. A three-dimensional computational method for blood flow in the heart. I. Immersed elastic fibers in a viscous incompressible fluid. *J. Comput. Phys.* 81:372–405

Powell BE. 1991 *Experimental measurements of flow through stenotic collapsible tubes.* MS thesis. Georgia Inst. of Tech. Atlanta

Reuderink PJ. 1991. *Analysis of the flow in a 3D distensible model of the carotid artery bifurcation. PhD dissertation.* Tech. Univ. of Eindhoven. Eindhoven, Netherlands.

Rodbard S. 1970. Negative feedback mechanisms in the architecture and function of the connective and cardiovascular tissues. *Perspect. Biol. Med.* 13:507–27

Rodkiewicz CM, Sinha P, Kennedy JS. 1990. On the application of a constitutive equation for whole blood. *J. Biomech. Eng.* 112:198–206

Salam TA, Lumsden AB, Suggs WD, Ku DN. 1996. Low shear stress promotes intimal hyperplasia thickening. *J. Vasc. Invest.* 2:12–22

Santamore WP, Bove AA, Carey RA. 1982. Tachycardia induced reduction in coronary blood flow distal to a stenosis. *Int. J. Cardiol.* 2:23–27

Shapiro AH. 1977. Steady flow in collapsible

tubes. *J. Biomech Eng.* 9:126–47
Siegel JM, Markou CP, Ku DN, Hanson SR. 1994. A scaling law for wall shear stress through an arterial stenosis. *J. Biomech. Eng.* 116:446–51
Siegel JM, Oshinski JN, Pettigrew RI, Ku DN. 1995. Comparison of phantom and computer-simulated MR images of flow in a convergent geometry: implications for improved two- dimensional MR angiography. *J. Magn. Reson. Imag.* 5:677–83
Strandness DE Jr, van Breda A, eds. 1994. *Vascular Diseases: Surgical and Interventional Therapy.* New York: Churchill Livingston
Tang TD. 1990. *Periodic flow in a bifurcating tube at moderate Reynolds number.* PhD dissertation. Georgia Inst. Tech., Atlanta
Taylor TW, Yamaguchi T. 1994. Three-dimensional simulation of blood flow in an abdominal aortic aneurysm-steady and unsteady flow cases. *J. Biomech. Eng.* 116(1):89–97
Womersley JR. 1955. Method for the calculation of velocity, rate of flow and viscous drag in arteries when their pressure gradient is known. *J. Physiol.* 127:553–63
Yoganathan AP, Lemmon JD Jr, Kim YH, Walker PG, Levine RA, Vesier CC. 1994. A computational study of a thin-walled three-dimensional left ventricle during early systole. *J. Biomech Eng.* 116:307–17
Young DF. 1979. Fluid mechanics of arterial stenoses. *J. Biomech. Eng.* 101:157–75
Yucel EK. 1994. Magnetic resonance angiography. In strandness & van Breda 1994, pp. 289–302
Zarins CK, Zatina MA, Giddens DP, Ku DN, Glagov S. 1987. Shear stress regulation of artery lumen diameter in experimental atherogenosis. *J. Vasc. Surg.* 5:413–20

Annual Review of Fluid Mechanics
Volume 29, 1997

CONTENTS